Journal of Alloys and Compounds 777 (2019) 1039–1043

Contents lists available at ScienceDirect

Journal of Alloys and Compounds

journal homepage: http://www.elsevier.com/locate/jalcom

Microwave dielectric properties of B and N co-doped SiC nanopowders prepared by combustion synthesis

Zi Yang [a], Zhimin Li [a, *], Tao Ning [a], Maolin Zhang [a], Yangxi Yan [a], Dongyan Zhang [a], Guozhong Cao [b]

[a] School of Advanced Materials and Nanotechnology, Xidian University, Xi'an, 710071, China
[b] Department of Materials Science and Engineering, University of Washington, Seattle, WA, 98195-2120, USA

ARTICLE INFO

Article history:
Received 17 April 2018
Received in revised form
31 October 2018
Accepted 6 November 2018
Available online 9 November 2018

Keywords:
SiC
Co-doping
Dielectric property
Microwave loss

ABSTRACT

B and N co-doped SiC nanopowders were prepared by combustion synthesis under a nitrogen atmosphere from the Si/C system, using α-Si_3N_4 powder and B powder as solid nitriding agent and dopant, respectively. The prepared particles had spherical morphology and narrow size distribution. XPS analysis demonstrated that B and N atoms successfully incorporated into SiC crystal and formed $Si_{1-x}B_xC_{1-y}N_y$ solid solution. Results of dielectric properties showed that the real part ε′ and imaginary part ε″ of the complex permittivities of the samples decreased first, and then increased with increasing N content. The sample with 5% B and 15% N revealed the greatest values in ε′ and ε″ and better microwave absorption performance. The corresponding mechanism of the dielectric properties of SiC improved by co-doping was discussed in detail.

1. Introduction

Recently, microwave absorbing materials have attracted widespread attention for civilian and military applications [1–4]. Microwave absorbing materials mean the materials that can dissipate the incident electromagnetic energy into heat. In terms of the microwave loss mechanism, microwave absorbing materials are usually divided into two types: magnetic absorbing materials and dielectric absorbing materials. The most commonly used materials include carbon-based materials [5–10], ferrites [11], magnetic metal particles [12,13], conductive polymers [14,15], and so on. However, with the development of electromagnetic defense and stealthy techniques, there are increasing requirements for microwave absorbing materials used at high temperature. Although a number of absorbers have been reported, most of these are unsuitable for high-temperature applications. Carbon-based absorbers such as carbon black, carbon nanotube, and graphene are easily oxidized at high temperatures, when they are exposed in air. For example, graphene materials have revealed high microwave absorption performance, but they have not been utilized at high temperature, limiting their further application [8–10]. Ferrites and magnetic absorbers have low Curie temperatures [16,17] and will become demagnetized at high temperature, thus degrading their microwave absorption performance. Additionally, conductive polymer absorbers will decompose at high temperature [18].

SiC is considered as one of the heat-resistant microwave absorbers, because of its good thermal stability and oxidation resistance, high strength and hardness [19]. However, the conductivity of SiC is low, and it has to be modified to tune in a certain range so as to enable to achieve high microwave absorbing property. The typical approach to increase conductivity is n-type doping (e.g. N doping) or p-type doping (e.g. Al and B doping). Jin et al. [20] reported Al-doped SiC powders that showed the doping availability on the dielectric property. Su et al. [21] prepared N-doped SiC powders by combustion synthesis, verifying that the dielectric property was improved via n-type doping. In addition, surface modification was reported to improve the microwave dielectric properties of SiC. Yang et al. [22] successfully covered ring-like NiO nanoparticles on the surface of SiC powders (NiO@SiC) by chemical deposition and oxidation, by which the dielectric loss tangent tanδ of SiC was greatly increased at 673 K.

In our previous research, we performed systematic studies on SiC absorbers by introducing impurity elements such as N and Al into SiC crystal lattice. The better dielectric loss properties were achieved by optimizing the compositions of dopants. Meanwhile, the influence of B doping on the dielectric property of SiC was

* Corresponding author.
E-mail address: lizhmin@163.com (Z. Li).

https://doi.org/10.1016/j.jallcom.2018.11.067
0925-8388/

studied [23–25]. However, for p-type doping, B doping has not significantly improved the dielectric properties of SiC compared to Al doping. Since it was restricted by solid solubility, only very small amounts of B could be incorporated into the SiC crystal. Yamamoto et al. [26] showed that the co-doping of Al and N could increase the N doping concentration in ZnO through calculating the band structure of ZnO. Wu et al. [27] also reported that co-doping of Mg and O would effectively enhance the Mg doping concentration in AlN. Similarly, if the co-doping ratio of donor to acceptor is reasonable, the dielectric properties of SiC doped with B are expected to be improved due to increasing solubility. Additionally, Straumal et al. [28] reported that the Co solubility could be increased with decreasing grain size in ZnO, so it is possible that the solubility of dopants might be increased for the nanosized SiC particle.

In this work, the nanosized SiC powders co-doped with B and N were prepared by combustion synthesis from Si/C/B/N system in N_2 atmosphere, and the effect of co-doping on the dielectric properties of SiC was investigated in detail. The mechanism of the dielectric properties improved by co-doping was discussed.

2. Experimental procedures

Silicon powder (99% in purity, mean particle size of 20 μm) and carbon black (99% in purity, mean particle size of 30 nm) were used as raw materials. Boron powder (99% in purity, mean particle size of 30 μm) and Si_3N_4 powder (99% in purity, mean particle size of 20 μm) were used as dopant and solid nitriding agent, respectively. And polytetrafluoroethylene (PTFE) powder (99.99% in purity, mean particle size of 75 μm) was used as chemical activator. The starting powders were weighed out in different molar ratios listed in Table 1. For comparison, the powder of Si/C was also weighed out in the molar ratio of $n_{Si}:n_C = 1:1$, in which B and N constituents were not contained. Then the powder batches were mixed in ethanol for 6 h and dried at 60 °C. Finally, the dried powders were put into a graphite crucible and calcined at the temperatures of 1400 °C in a resistance heating graphite furnace, with a heating rate of 10 °C/min in a 0.1 MPa N_2 atmosphere.

The crystalline phases of the as-prepared powders were identified by X-ray diffractometer (XRD, D8 Advance, Bruker, Germany), using Cu K_α radiation. The morphologies of the powders were observed by field emission scanning electron microscopy (FESEM, JSM-7500F, JEOL, Japan). X-ray photoelectron spectroscopy (XPS, K-Alpha, Thermo Scientific) was performed for determining the compositions. The dielectric parameters at room temperature were determined in the frequency range of 8.2–12.4 GHz using a PNA network analyzer (Agilent Technologies E8362B, Palo Alto, CA). The samples were prepared by mixing the powders with molten paraffin in a mass ratio of 1:4, and then the mixtures were molded into a brass flange to fabricate rectangular composite samples with the dimension of 10.16 mm (width) × 22.86 mm (length) × 2.00 mm (thickness).

The microwave absorption performance of the SiC powders was investigated. To characterize the microwave absorption performance, we calculated the parameters of reflection loss (RL) of the samples, which were determined by the following Eqs. (1)–(3) [29–31]:

$$RL = 20log\left|(Z_{in} - Z_0)/(Z_{in} + Z_0)\right| \quad (1)$$

$$Z_0 = \sqrt{\mu_0/\varepsilon_0} \quad (2)$$

$$Z_{in} = Z_0\sqrt{\mu_r/\varepsilon_r}\tanh\left[j\frac{2\pi}{c}\sqrt{\mu_r\varepsilon_r}fd\right] \quad (3)$$

where Z_{in} is the input impedance of the coating, Z_0 is the impedance of free space, ε_r and μ_r are the relative complex permittivity and permeability, respectively, f is the frequency of the electromagnetic wave, d is the thickness of the coating, and c is the velocity of light. In this study, the μ_r is equal to 1 due to the fact that SiC is a nonmagnetic material.

Table 1
The molar ratios of elements in the samples.

Samples	Molar ratios				PTFE (wt%)
	B	Si	C	N	
SiC	0	1	1	0	20%
5% B and 5% N-doped SiC	0.05	0.95	0.95	0.05	20%
5% B and 15% N-doped SiC	0.05	0.95	0.85	0.15	20%

3. Results and discussion

Fig. 1 shows the XRD patterns of the undoped and co-doped SiC powders synthesized by combustion synthesis. As can be seen, the peaks of β-SiC phase are dominant in both the undoped and co-doped powders. There is no any impurity peak of B compounds, but the weak diffraction peak of C appears in all the samples. This is because that a depolymerization reaction occurs between Si and PTFE, and the product contains a small amount of C, as shown in Eq. (4) [32]:

$$Si(s) + (C_2F_4)_n(s) \rightarrow SiF_4(g) + 2C(s) \quad (4)$$

In addition, the diffraction peaks of α-SiC phase appear in the powders. The peaks are caused by the stacking fault defects of SiC. In contrast, for doped powders, the diffraction peaks of α-Si_3N_4 phases are present, and the intensity of characteristic peaks increases with increasing N content. As the surface of the particles was partially oxidized in the synthesis process, a trace amount of SiO_2 was generated in the samples.

FESEM images of the as-prepared powders are shown in Fig. 2. As can be seen from the photographs, all the powders are nanosized particles. The particles have spherical morphology and narrow size

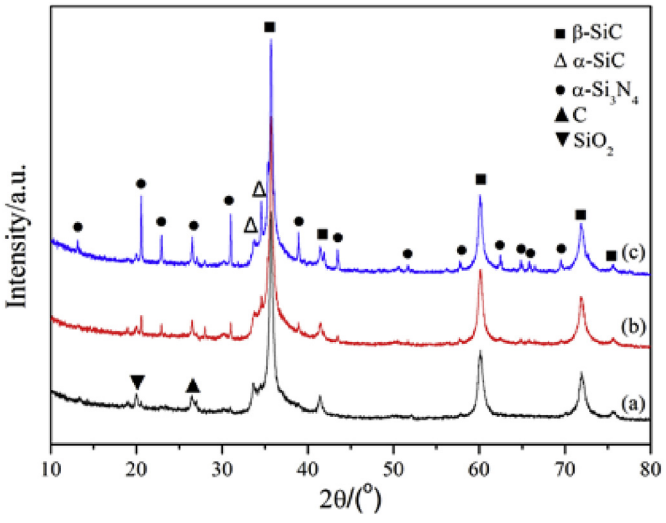

Fig. 1. XRD patterns of the powders synthesized with different N contents: (a) undoped SiC; (b) 5% B and 5% N co-doped SiC; (c) 5% B and 15% N co-doped SiC.

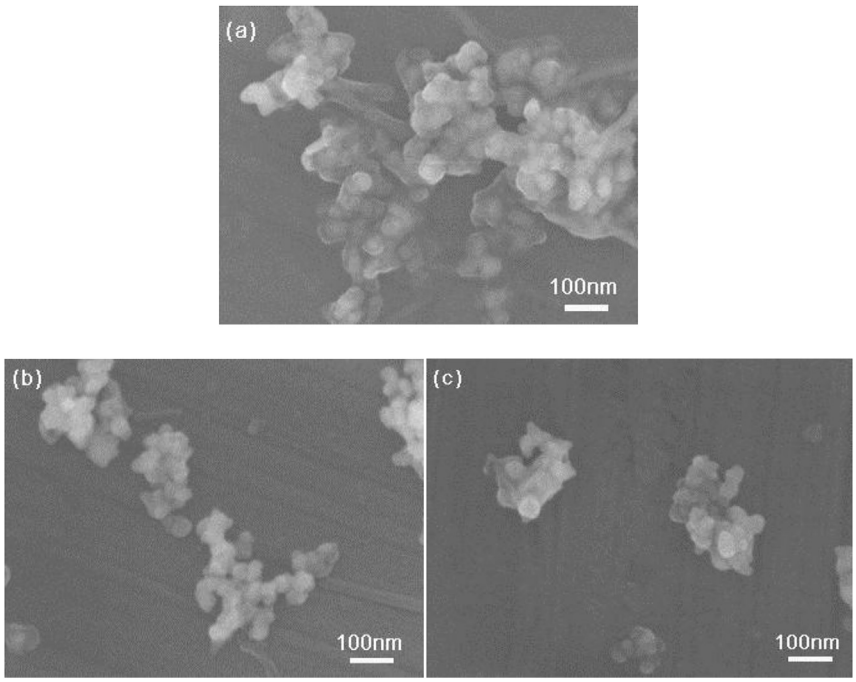

Fig. 2. FESEM images of the powders synthesized with different N contents: (a) undoped SiC; (b) 5% B and 5% N co-doped SiC; (c) 5% B and 15% N co-doped SiC.

distribution. It also can be seen that the size of the doped powders is less than the undoped powder. In the case of 5% B and 15% N doping, the average particle size of the prepared powder is about 30 nm. Martin et al. [33] also reported that B doping could cause SiC particle size to decrease in synthesis process. In this study, B and N atoms entered into the SiC lattice and would hinder the growth of SiC crystallite, leading to the decrease of the particle size of doped SiC powders.

In order to verify whether the prepared B and N co-doped SiC nanopowders were $Si_{1-x}B_xC_{1-y}N_y$ solid solution, the XPS was performed for the 5% B and 15% N co-doped powder, as shown in Fig. 3. One can see that the sample contains B and N elements, besides Si and C elements. The C 1s peaks appear at 283.48 eV, 284.08 eV, and 284.78 eV, which represent C–Si, C–C, and C–O bonds, respectively. The formation of C–O bonds may be from nitrogen gas impurity or insufficiently high vacuum pressure in the furnace. The C–C bonds are primarily caused by the presence of sp^2C and sp^3C in SiC crystal.

As shown in the Si 2p spectrum of the prepared powder and its Gaussian fitting curves in the Fig. 3(b), the sample consists of the peaks located at 100.52 eV, 101.7 eV, and 103.08 eV, which represent Si–N, Si–C, and Si–O bonds, respectively. As aforementioned, the surface of the particles was partially oxidized, resulting in the formation of some Si–O bonds in the sample. The N 1s spectrum indicates that it is composed mainly of the peaks at 397.1 eV and 397.9 eV, which are N–N and N–SiC bonds, respectively [34]. Thus, it is concluded that N atoms incorporate into the SiC crystal and form SiC/N solid solutions. Since the powder was synthesized in a nitrogen atmosphere, the surface adsorbed nitrogen, leading to the presence of N–N bonds. From Fig. 3(d), it can be seen that there is only one B 1s peak located at 192.2 eV, while the standard B 1s peak locates at 189.1 eV. This is because the electronegativity of C atom is greater than that of B atom, which causes the peak to shift towards higher energy by 1.1 eV, indicating that B atoms are present in the SiC lattice [35,36]. Based on the above results and analysis, it is confirmed that both B and N atoms incorporate into the SiC crystal and form the $Si_{1-x}B_xC_{1-y}N_y$ solid solution, hence leading to the generation of holes and electrons in the crystal which arise from B_{Si} and N_C point defects, respectively. When the external field changes, these holes and electrons in the SiC crystal have to overcome a certain potential barrier to keep reciprocating, which causes the relaxation polarization and loss [37].

The complex permittivities of the undoped and doped SiC powders in the frequency range of 8.2 GHz–12.4 GHz are shown in Fig. 4. It can be seen that the values of real part ε' and imaginary part ε'' decrease firstly, and then increase with increasing N content. Among all the samples, the one doped with 5% B and 15% N reveals the greatest values in ε' and ε'', which are 5–5.2 and 1–1.1, respectively, and have a significant increase compared to the undoped one. Thus, the values of ε' and ε'' can be tailored by the doping ratio of N to B.

The solid nitriding agent of Si_3N_4 has a high decomposition temperature (>1900 °C). In the synthesis process, the Si_3N_4 decomposed to generate a large amount of N_2, which would cause a high local pressure. The high local pressure of N_2 enabled N atoms easily to enter the SiC crystal and substitute on C atoms due to their similar atomic radii and electronegativities, forming N_C point defects. As mentioned above, under an alternating external field at GHz frequencies, the weakly bound free electrons around N_C point defects have to overcome a certain potential barrier to keep reciprocating, which leads to electron relaxation polarization and loss, and increases the values of ε' and ε''. When the B dopant was simultaneously added, the electrons from N_C point defects would be annihilated with the holes from B_{Si} point defects formed by the replacement of B atoms on Si atoms in SiC crystal, contributing to the decrease in ε' and ε'' [38]. The sample with 5% B and 5% N has lower ε' and ε'' than undoped SiC. It suggests that the co-doping approach gives rise to the increase of B solubility in SiC crystal, and that the more amount of solute B sufficiently offsets the contribution to ε' and ε'' from N_C point defects. When the amount of Si_3N_4 reaches to 15%, more N_C point defects result in the greater values of ε' and ε'' for the sample.

The microwave absorption performances of SiC samples were investigated. In this study, according to Eq. (1), we calculated the

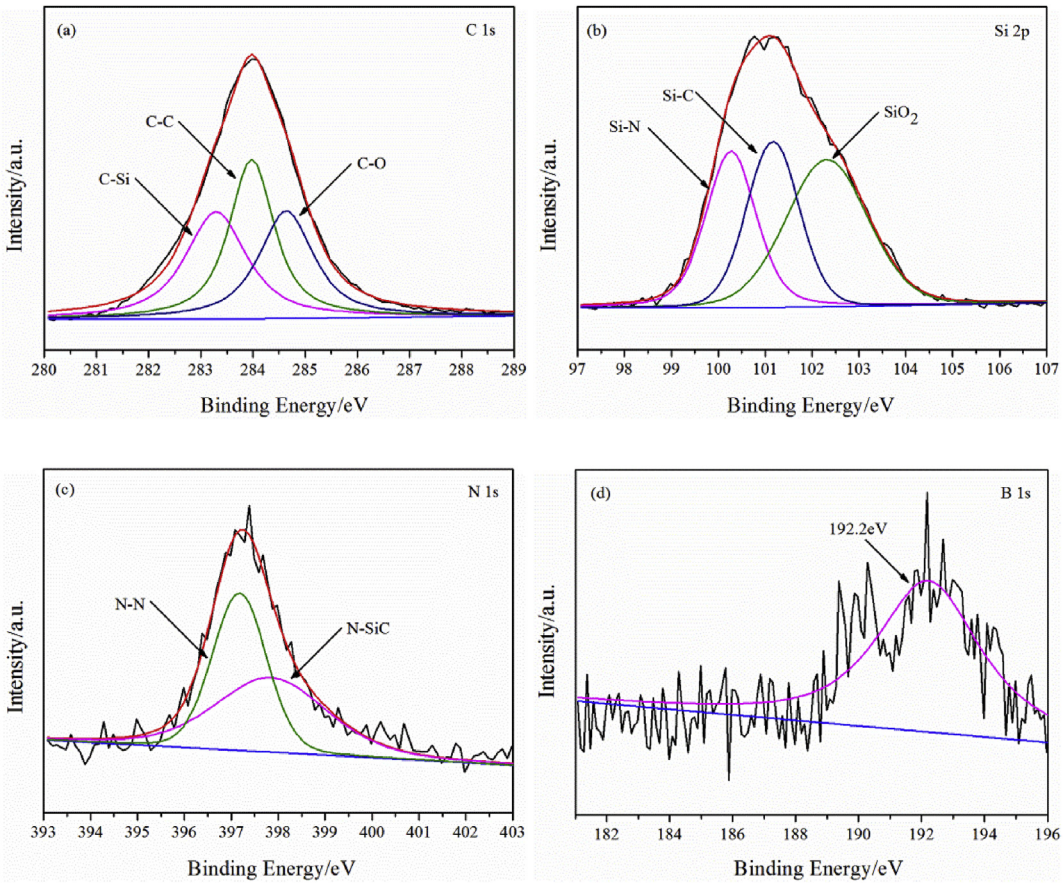

Fig. 3. XPS spectra of 5% B and 15% N co-doped SiC powder.

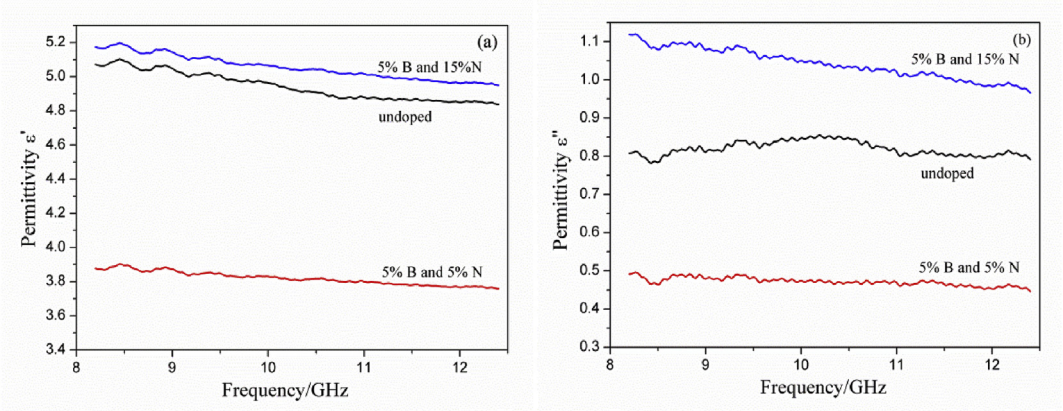

Fig. 4. Real part ε' and imaginary part ε'' of permittivity for the samples synthesized with different N contents.

reflection loss of the 5% B and 15% N doped sample at different coating thicknesses, and found that the sample revealed the better reflection loss in the case of 3.9 mm thickness. Fig. 5 shows the reflection loss of the undoped and doped SiC samples with the coating thickness of 3.9 mm. It can be seen that the variation tendency of the reflection loss is consistent with the permittivity for SiC samples. The reflection loss of the SiC sample is significantly improved by 5% B and 15% N doping, with the lowest value of −7.6 dB at 9.3 GHz.

Attenuation constant (α) is a parameter to reflect the dissipation capacity of microwave absorbing materials for electromagnetic wave, which can be given by the Eq. (5) [39].

$$\alpha = \frac{\sqrt{2}\pi f}{c}\sqrt{\mu''\varepsilon'' - \mu'\varepsilon' + \sqrt{\left(\mu'^2 + \mu''^2\right)\left(\varepsilon'^2 + \varepsilon''^2\right)}} \tag{5}$$

Fig. 6 shows the attenuation constant of the samples synthesized with different N contents. As can be seen, the attenuation constant of undoped sample is 31–47 Np/m (Np is the abbreviation of neper) in the frequency range of 8.2–12.4 GHz, and it reaches to 42–57 Np/m for the 5% B and 15% N doped sample. The greater attenuation constant implies a higher dissipation capacity of

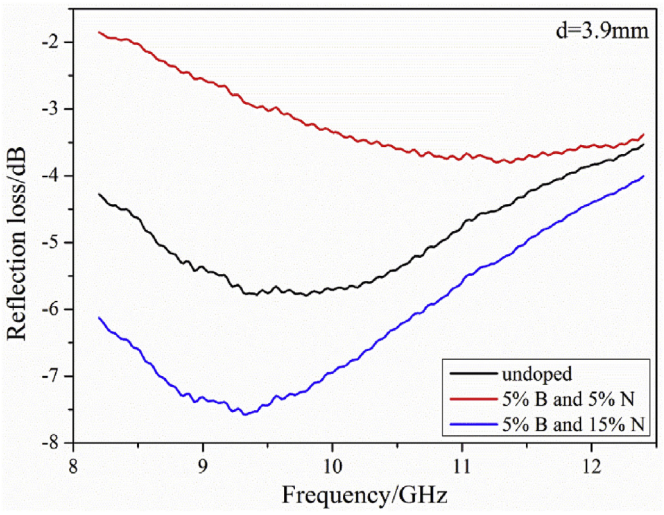

Fig. 5. Reflection loss of the samples synthesized with different N contents.

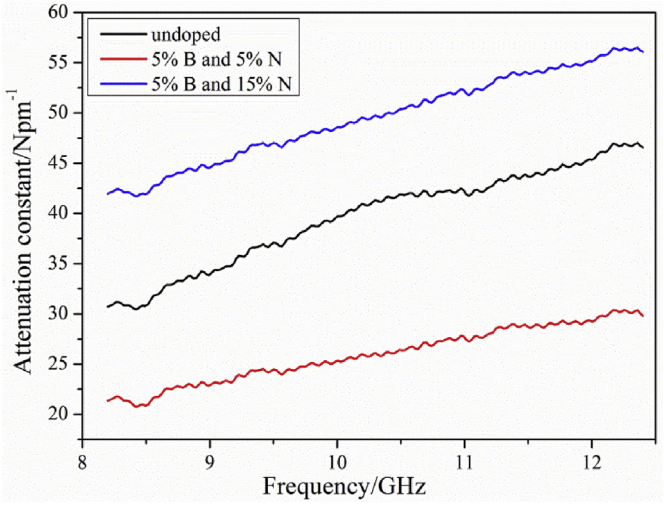

Fig. 6. Attenuation constant of the samples synthesized with different N contents.

microwave absorbing materials for electromagnetic wave [40]. Therefore, the greatest value of attenuation constant for 5% B and 15% N doped sample further demonstrates that the better microwave absorption performance is attributed to the holes or electrons arising from doping defects in the crystal.

4. Conclusions

In this study, B and N co-doped SiC nanopowders were prepared by combustion synthesis. Results showed that the β-SiC major phases were generated in the case of B and N co-doping. The powders revealed spherical morphology and narrow size distribution. When the doping content was 5% B and 15% N, the average particle size of the prepared powder was about 30 nm. It was further proved by XPS that the $Si_{1-x}B_xC_{1-y}N_y$ solid solution was formed because of the substitution of B atoms on Si atoms and N atoms on C atoms in SiC crystal. The complex permittivities of the undoped and co-doped SiC samples in the frequency range of 8.2 GHz–12.4 GHz were determined. Results showed that B and N co-doping could tailor the dielectric properties of SiC. The 5% B and 15% N co-doped SiC sample revealed the greatest values in ε' and ε'' which were 5–5.2 and 1–1.1, respectively, arising from more N_C point defects. Also, it showed the greatest values in both the microwave reflection loss and attenuation constant among all the samples.

Acknowledgements

Authors would like to acknowledge the financial supports of National Natural Science Foundation of China (Nos. 51701147, 61701369 and 51602240), and Natural Science Basic Research Plan in Shaanxi Province of China (No. 2018JM5060).

References

[1] L. Zhang, V. Hessel, J. Peng, Chem. Eng. J. 332 (2018) 131–139.
[2] Y. Qing, D. Min, Y. Zhou, F. Luo, W. Zhou, Carbon 86 (2015) 98–107.
[3] Y. Liu, Y. Li, F. Luo, X. Su, J. Xu, J. Wang, X. He, Y. Qu, J. Alloys Compd. 715 (2017) 21–28.
[4] J. Liu, W.Q. Cao, H.B. Jin, J. Yuan, D.Q. Zhang, M.S. Cao, J. Mater. Chem. C 3 (2015) 4670–4677.
[5] E. Sano, E. Akiba, Carbon 78 (2014) 463–468.
[6] B. Wen, M.S. Cao, Z.L. Hou, W.L. Song, L. Zhang, M.M. Lu, H.B. Jin, X.Y. Fang, W.Z. Wang, J. Yuan, Carbon 65 (2013) 124–139.
[7] M.S. Cao, W.L. Song, Z.L. Hou, B. Wen, J. Yuan, Carbon 48 (2010) 788–796.
[8] B. Wen, M. Cao, M. Lu, W. Cao, H. Shi, J. Liu, X. Wang, H. Jin, X. Fang, W. Wang, J. Yuan, Adv. Mater. 26 (2014) 3484–3489.
[9] W.Q. Cao, X.X. Wang, J. Yuan, W. Wang, M.S. Cao, J. Mater. Chem. C. 3 (2015) 10017–10022.
[10] Y. Zhang, X. Wang, M. Cao, Nano Res. 11 (2018) 1426–1436.
[11] J. Shen, K. Chen, L. Li, W. Wang, Y. Jin, J. Alloys Compd. 615 (2014) 488–495.
[12] D. Zheng, T. Liu, L. Zhou, Y. Xu, J. Magn. Magn. Mater. 419 (2016) 119–124.
[13] Y.B. Feng, T. Qiu, C.Y. Shen, J. Magn. Magn. Mater. 318 (2007) 8–13.
[14] Y. Yang, J. Wang, Mater. Lett. 124 (2014) 151–154.
[15] Y. Xu, L. Yuan, J. Cai, D. Zhang, J. Magn. Magn. Mater. 343 (2013) 239–244.
[16] S.H. Hosseini, S.H. Mohseni, A. Asadnia, H. Kerdari, J. Alloys Compd. 509 (2011) 4682–4687.
[17] S.W. Phang, T. Hino, M.H. Abdullah, N. Kuramoto, Mater. Chem. Phys. 104 (2007) 327–335.
[18] J.H. Oh, K.S. Oh, C.G. Kim, C.S. Hong, Compos. Part B-Eng. 35 (2004) 49–56.
[19] B. Zhang, J. Li, J. Sun, S. Zhang, H. Zhai, Z. Du, J. Eur. Ceram. Soc. 22 (2002) 93–99.
[20] H.B. Jin, M.S. Cao, W. Zhou, S. Agathopoulos, Mater. Res. Bull. 45 (2010) 247–250.
[21] X. Su, W. Zhou, F. Luo, Z. Li, D. Zhu, J. Alloys Compd. 476 (2009) 644–647.
[22] H. Yang, M. Cao, Y. Li, H. Shi, Z. Hou, X. Fang, H. Jin, W. Wang, J. Yuan, Adv. Opt. Mater. 2 (2014) 214–219.
[23] Z. Li, W. Zhou, X. Su, Y. Huang, G. Li, Y. Wang, J. Am. Ceram. Soc. 92 (2009) 2116–2118.
[24] Z. Li, W. Zhou, X. Su, F. Luo, Y. Huang, C. Wang, J. Alloys Compd. 509 (2011) 973–976.
[25] Z. Li, W. Zhou, T. Lei, F. Luo, Y. Huang, Q. Cao, J. Alloys Compd. 475 (2009) 506–509.
[26] T. Yamamoto, H. Katayamayoshida, Jpn. J. Appl. Phys. 38 (1999) L166–L169.
[27] R.Q. Wu, L. Shen, M. Yang, Z.D. Sha, Y.Q. Cai, Y.P. Feng, Z.G. Huang, Q.Y. Wu, Phys. Rev. B 77 (2008), 073203.
[28] B.B. Straumal, A.A. Mazilkin, S.G. Protasova, A.A. Myatiev, P.B. Straumal, B. Baretzky, Acta Mater. 56 (2008) 6246–6256.
[29] C. Qiang, J. Xu, Z. Zhang, L. Tian, S. Xiao, Y. Liu, P. Xu, J. Alloys Compd. 506 (2010) 93–97.
[30] L. Zhang, H. Zhu, Mater. Lett. 63 (2009) 272–274.
[31] H. Wu, L. Wang, S. Guo, Z. Shen, Appl. Phys. A 108 (2012) 439–446.
[32] G.L. Khachatryan, A.B. Arutyunyan, S.L. Kharatyan, Combust. Explos. Shock Waves 42 (2006) 543–548.
[33] H.P. Martin, E. Muller, G. Irmer, F. Babonneau, J. Eur. Ceram. Soc. 17 (1997) 659–666.
[34] A. Vijayakumar, R.M. Todi, K.B. Sundaram, J. Electrochem. Soc. 154 (2007) 281–306.
[35] Y. Taiima, W.D. Kingery, J. Am. Ceram. Soc. 65 (1982) C27–29.
[36] M. Han, X. Yin, W. Duan, S. Ren, L. Zhang, L. Cheng, J. Eur. Ceram. Soc. 36 (2016) 2695–2703.
[37] D. Zhao, H. Zhao, W. Zhou, Phys. E 9 (2001) 679–685.
[38] P.L. Zhou, S.K. Zheng, Y. Tian, S.M. Zhang, R.Q. Shi, J.F. He, X.B. Yan, Acta Phys. Sin. 63 (2014) 053102–053191.
[39] Y. Liu, X. Su, F. Luo, J. Xu, J. Wang, X. He, Y. Qu, Ceram. Int. 44 (2018) 1995–2001.
[40] M. Cao, X. Wang, W. Cao, X. Fang, B. Wen, J. Yuan, Small 14 (2018) 1800987.